Energy-Band Structures of Cd_3As_2 and Zn_3As_2

P. J. LIN-CHUNG
Naval Research Laboratory, Washington, D. C. 20390
(Received 8 July 1969)

The energy-band structures of Cd_3As_2, Zn_3As_2, and $Cd_{1.2}Zn_{1.8}As_2$ in a hypothetical fluorite structure have been determined, employing the pseudopotential method. From these results a qualitative picture of the band-edge structure in real crystals is deduced. It is shown that many optical and transport phenomena can be interpreted using these energy-band structures.

I. INTRODUCTION

In recent years there has been a growing interest in the II-V compounds Cd_3As_2, Zn_3As_2, etc., based on the possible occurrence of either small energy gaps or extremely high electronic mobilities and low-electron effective masses or a combination of such properties. In previous works, the interpretation of experimental results has been hampered by the lack of band calculation that would serve to establish the positions and shapes of the valence and conduction-band edges. A theoretical determination of the band structures of these substances, on the other hand, faces many significant difficulties.

The major difficulty in a theoretical work originates from the exceptionally complicated crystal structure of these substances. Recently, x-ray analysis[1] has shown that the Cd_3As_2-type compounds crystallize in a body-centered tetragonal structure with 32 As ions and 48 Cd ions per unit cell. Its space group belongs to $C_{4v}^{12}(I4_1cd)$. Such a large unit cell introduces a large number of valence electrons (256 valence electrons per unit cell) and a very involved structure factor. An accurate determination of such a large number of valence bands would require the inclusion of a large number of terms in the expansion of orthogonalized-plane-wave (OPW) wave functions in order to ensure the convergence of the calculation. For example, the InAs crystal has only eight valence electrons per unit cell, yet approximately 90 plane waves should be included in the expansion of the Bloch-wave function to give a reasonably well-convergent result. Thus, in the Cd_3As_2 case, one is inevitably confronted with solving secular determinants of the order of 1000, which at the present time requires astronomical computer time. The complexity of the structure factor as well as the computational difficulties in finding a self-consistent crystal potential also makes the theoretical study virtually impossible.

To obviate the difficulty in finding a self-consistent potential, we seek recourse to the pseudopotential method which has been so useful in other band calculations of simpler materials. Frequently, the weak pseudopotentials obtained for the elements or compounds are taken over to construct the weak pseudopotentials for other compounds. Since the pseudopotential of an atom in one substance does not differ much from that of the same atom in another substance, the previously determined local atomic pseudopotential with volume correction factors could equally well be adapted in our investigations of the II-V compounds. Indeed, band calculations have already been carried out for the pure cadmium, zinc,[2] and arsenic.[3] These calculations provide us with the pseudopotential form factors for atomic Cd, Zn, and As. These atomic pseudopotentials are particularly useful since they have been so accurately determined. As pointed out in Ref. 2, the band structures resulting from the pseudopotential scheme give extremal cross-sectional areas of the Fermi surfaces of cadmium and zinc consistent with de Haas–van Alphen measurements and all other reported measurements of the Fermi surface properties. In particular, a purely local pseudopotential approach resulted in average errors that were only of the order of 10^{-2} Ry in Zn and 10^{-3} Ry in Cd, when the error in the calculations is expressed as the necessary shift in the Fermi energy to bring the theoretically calculated de Haas–van Alphen frequencies into exact agreement with experiment.

In the second step towards overcoming the computational difficulties, we are forced to make approximations to the crystal structure. The Cd_3As_2 crystal may be viewed as a fluorite crystal structure with cadmium-ion vacancies distributed periodically throughout the crystal. The effect of the vacancies on the valence electrons is then taken into account by a vacancy pseudopotential which is the negative of the cadmium atomic pseudopotential. For convenience, we assume the vacancies distributed in such a way that their existence is accounted for by an effective vacancy potential superimposed on the cadmium atomic pseudopotential presented in the ideal fluorite structure. This assumption, on the one hand, gives a reasonable physical picture of the potential field seen by a valence electron and, on the other hand, allows us to formulate the Schrödinger equation for manageable computation. The present work is exploratory in character. Our aim is not to seek complete agreement with experiment. Our choice of the hypothetical structure will be too crude for that. Rather, we seek to simply understand

[1] G. A. Steigman and J. Goodyear, Acta Cryst. **B24**, 1062 (1968).

[2] R. W. Stark and L. M. Falicov, Phys. Rev. Letters **19**, 795 (1967).

[3] P. J. Lin and L. M. Falicov, Phys. Rev. **142**, 441 (1966).

the general nature of the results employing the atomic pseudopotentials for each constituent atom presently available. Since a band-structure calculation for Cd_3As_2 crystal in its real structure will not be possible in the foreseeable future, this work, hopefully, would provide information as to probable locations and shapes of valence and conduction band edges.

In Sec. II we shall describe the crystal structures of these compounds and analyze the relationships between the real and hypothetical crystal structures. In Sec. III we define the potentials relevant to both structures and present the Schrödinger equation used in our formal calculations. The results of our numerical computation are given in Sec. IV. From these results we are able to deduce a qualitative picture of the band-edge structures of these compounds in their real crystal structures and to understand the presently available experimental data. A detailed discussion of the essential changes in the energy-band structures as one goes from the hypothetical to the real structures will be given in Sec. V. A comparison of the results with experimental data is also to be found there.

II. CRYSTAL STRUCTURE

The crystal structure of Cd_3As_2 was determined recently by Steigmann and Goodyear[1] as body-centered tetragonal with 80 atoms per unit cell. This structure, as well as many others, can be well understood by a diagram looking down along the c axis. A most convenient way to illustrate this structure is to divide the unit cell along the c axis by eight equally spaced planes, representing atoms on the planes as circles and atoms at $\Delta z=c/16$ below the planes as crosses. This diagram is given in Fig. 1, where Cd atoms are on the planes and As atoms are below.

Examination of Fig. 1 shows that each Cd atom is tetrahedrally coordinated with arsenic atoms as their nearest neighbors, while each As atom is surrounded by Cd atoms located at six of the eight corners of a cube, the two vacant sites being at diagonally opposite corners of a cubic face.

The space group of the structure given in Fig. 1 actually belongs to $C_{4v}^{12}(I4_1cd)$ with a body-centered tetragonal Bravais lattice. This space group is nonsymmorphic; some of its symmetry operations are associated with nonprimitive translations. There are several alternative methods of describing this space group, each one of which places the origin at a specific location. If the origin is chosen to be at the As atom 0, as indicated in Fig. 1, the symmetry operations of the factor group which carries us from one atom in the environment of 0 to its equivalent atoms are listed in Table I. The operations L_1 to L_8 carry the Cd (As) atoms labeled by 1, 2, 3, etc., to atoms with the same labels. The As atoms are themselves in a cubic close-packed structure. The x-ray analysis[1] indicates that the As atoms are slightly displaced from their positions in a cubic close-packed array. The displacement is small, being 0.05 Å as compared with the lattice constants shown in Table II. We shall therefore ignore such small deviations. The Cd atoms were found to displace 0.25 Å from their positions in Fig. 1 towards neighboring vacant sites, causing a variation of the bond lengths within each Cd-As tetrahedron. As a result of these displacements, atoms with different labels will no longer be at equivalent sites. The space group, however, remains $C_{4v}^{12}(I4_1cd)$, whose factor group contains operations L_1 to L_8 only.

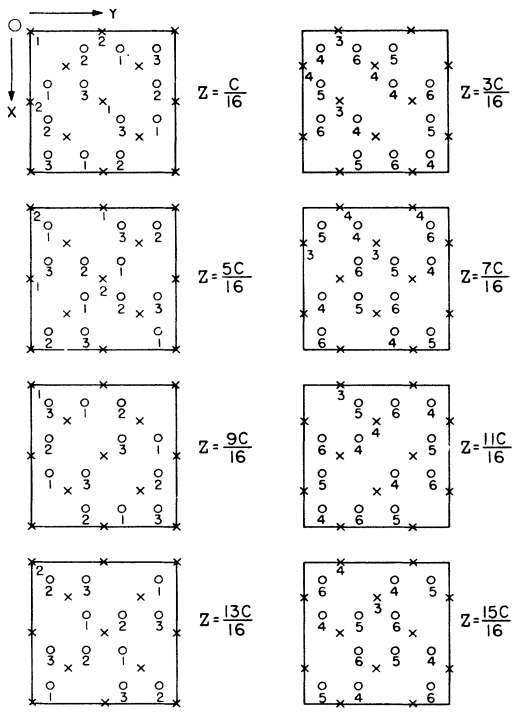

FIG. 1. Idealized crystal structure of Cd_3As_2-type crystals. The unit cell is divided by eight equally spaced planes along the z direction. As atoms are represented by crosses at $\Delta z=\frac{1}{16}c$ below each plane and Cd atoms are represented by circles on each plane.

It is interesting to see how a fluorite structure can be formed by simply filling the vacant sites in Fig. 1 with Cd atoms. After the vacant sites are filled, the unit cell in Fig. 1 will transform into 16 equivalent fluorite unit cells with the As^{3-} replacing the Ca^{2+}

TABLE I. Elements of the factor group C_{4v}^{12} ($s=1$ to $s=8$), where $t_A=\frac{1}{2}a\hat{\imath}$, $t_B=\frac{1}{2}a\hat{\jmath}$, $t_c=\frac{1}{4}c\hat{k}$.

S	Class	Operation L_s	$L_s^{-1}\mathbf{r}$		
1	E	$(I,0)$	x	y	z
2	C_4^2	$(\delta_{2z},0)$	$\bar{x}$	$\bar{y}$	z
3	C_4	(δ_{4z},t_B+t_c)	y	$\bar{x}+\frac{1}{2}a$	$z+\frac{1}{4}c$
4		$(\delta_{4z}^{-1},t_B+t_c)$	$\bar{y}$	$x+\frac{1}{2}a$	$z+\frac{1}{4}c$
5	σ_v	$(\rho_y,2t_c)$	x	$\bar{y}$	$z+\frac{1}{2}c$
6		$(\rho_x,2t_c)$	$\bar{x}$	y	$z+\frac{1}{2}c$
7	σ_d	$(\rho_{x\bar{y}},t_A+t_c)$	$\bar{y}+\frac{1}{2}a$	$\bar{x}$	$z+\frac{1}{4}c$
8		(ρ_{xy},t_A+t_c)	$y+\frac{1}{2}a$	x	$z+\frac{1}{4}c$

TABLE II. Quantities used in the calculations.

		Cd_3As_2	Zn_3As_2	$Cd_{1.2}Zn_{1.8}As_2$
Lattice constants (Å)	a	12.67[a]	11.783[b]	8.61[b]
	c	25.48[a]	23.652[b]	12.05[b]
Hypothetical fluorite structure lattice constants A (in a.u.)		11.98	11.14	11.45
Volume per primitive cell of fluorite structure		429.35	345.34	375.28
Pseudopotentials form factors (Ry)				
$V(111)$		−0.1194	−0.1304	−0.1212
$V(200)$		−0.0680	−0.0760	−0.0530
$V(220)$		−0.0094	0.0082	0.0104
$V(113)$		0.0150	0.0246	0.0213
$V(222)$		0.0056	0.0110	0.0033
$V(400)$		0.0134	0.0050	0.0077
$V(331)$		0.0022	0	0
$V(420)$		0.0010	0	0

[a] G. A. Steigmann and J. Goodyear, Acta Cryst. **B24**, 1062 (1968).
[b] W. Zdanowicz, K. Lukaszewicz, and W. Trzebiatowski, Bull. Acad. Polon. Sci. **12**, 169 (1964).

and the Cd^{2+} replacing F^- in a calcium-fluoride structure. The new unit cell, being much simpler than the original one, contains only three basis atoms. As indicated in Fig. 2(a), the dashed lines and the planes $z=\frac{1}{4}nc$, $z=\frac{1}{4}(n+1)c$ form the boundary of the fluorite unit cell with lattice constant equal to $\frac{1}{2}a$.

In order to illustrate more explicitly the difference between Figs. 1 and 2(a), we display the arrangement of the vacant sites in Fig. 2(b), in which the real unit cell is divided into four sections along the c axis. The tail and head of the arrow are situated at the upper and lower vacant sites, respectively, along the body diagonal of each small fluorite unit cell. Note that there are only four types of small cubes containing four differently oriented arrows. In the environment of an arsenic atom, the vacancies arrange themselves in such a pattern

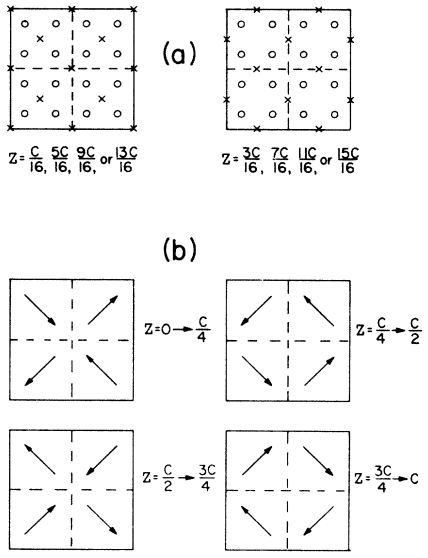

FIG. 2. Relation of (a) the fluorite structure and (b) the cadmium vacant-site structure to the Cd_3As_2 structure given in Fig. 1. The circles are Cd atoms on each plane, the crosses are As atoms at $\Delta z=\frac{1}{16}c$ below each plane. Broken line indicates the base boundary of fluorite unit cell. The tail and head of each arrow are situated at the upper and lower vacant sites, respectively, along the body diagonal of each small unit cube.

that along any direction, there is always equal probability in finding each type of small cube. This infers that, as far as the As atoms are concerned, they feel a vacancy potential field that is equal to the average of the fields produced by the vacancies in a structure containing solely one type of small cube. This is a reasonable first approximation because, as mentioned before, the cadmium atoms actually tend to displace towards the vacancy sites and hence the vacancy potentials resulting from an "averaged" treatment should be more realistic than the one from an "exact" treatment.

Let us now consider the structures in the momentum space. The reciprocal lattices of the real and fluorite structures are identical to those of the body-centered tetragonal and fcc structures, respectively. The basis reciprocal lattice vectors have the following forms:

$$\begin{aligned}&\mathbf{b}_1=(2\pi/a)(1,1,0),\\ &\mathbf{b}_2=(2\pi/a)(0,1,\tfrac{1}{2}),\\ &\mathbf{b}_3=(2\pi/a)(1,0,\tfrac{1}{2}),\end{aligned}\qquad \text{for real structure with the condition } c=2a, \tag{2.1}$$

and

$$\begin{aligned}&\mathbf{b}_1'=(4\pi/a)(1,1,\bar{1}),\\ &\mathbf{b}_2'=(4\pi/a)(\bar{1},1,1),\\ &\mathbf{b}_3'=(4\pi/a)(1,\bar{1},1),\end{aligned}\qquad \text{for fluorite structure.} \tag{2.2}$$

Throughout this paper a and c always refer to the lattice parameters for the real structure.

In terms of these basis vectors, the corresponding reciprocal lattice vectors (RLV) are expressed as $\mathbf{G}=(n_1\mathbf{b}_1+n_2\mathbf{b}_2+n_3\mathbf{b}_3)$ and $\mathbf{G}'=(n_1\mathbf{b}_1'+n_2\mathbf{b}_2'+n_3\mathbf{b}_3')$ with n_1, n_2, n_3 representing any integers. Or equivalently,

$$\mathbf{G}=(2\pi/a)(l_1,l_2,l_3), \tag{2.3}$$

where

$$\begin{aligned}&l_3=\text{half integers},\\ &l_1(l_2)=\text{even integers},\\ &l_2(l_1)=\text{odd integers},\end{aligned}$$

or

$$l_3 = \text{integers},$$

l_1 and l_2 = both even or both odd integers,

and

$$\mathbf{G}' = (4\pi/a)(l_1', l_2', l_3'), \tag{2.4}$$

where l_1', l_2', and l_3' are all even or all odd integers.

The Brillouin-zone geometries for these two reciprocal lattices are shown in Fig. 3. We want to point out that the first Brillouin-zone volume of the real structure is only $\frac{1}{16}$th that of the fluorite structure. Recall that in three dimensions the wave vectors $\mathbf{k}$ and $\mathbf{k}+\mathbf{G}$ are considered to be equivalent if $\mathbf{G}$ is any reciprocal lattice vector (RLV) of the reciprocal space. In addition, a small potential with nonzero Fourier component $V_{\mathbf{G}}$ will mix states which have wave numbers differing by $\mathbf{G}$.

If we examine Eqs. (2.3) and (2.4) carefully, all allowed $\mathbf{G}'$ values are also allowed RLV of the real structure. On the contrary, we can find many $\mathbf{G}$ that are not RLV of the fluorite structure. As a consequence, an extra potential, with the symmetry of the real structure, acting on the electrons in the fluorite structure will mix states with wave numbers differing by $\mathbf{G}$. For example, the states associated with the following points in momentum space will be mixed:

(1) $X = (4\pi/a)(1,0,0)$ mixed with $\Gamma = (4\pi/a)(0,0,0)$,

(2) $(4\pi/a)(\delta,0,0)$ mixed with $(4\pi/a)(1-\delta, 0, 0)$, where $\delta \leq 1$,

(3) $(4\pi/a)(\delta,\delta,0)$ mixed with $(4\pi/a)(1-\delta, 1-\delta, 0)$, where $\delta \leq 1$,

(4) $L = (4\pi/a)(\frac{1}{2},\frac{1}{2},\frac{1}{2})$ mixed with $(4\pi/a)(0,0,\frac{1}{2})$ and $(4\pi/a)(\frac{1}{2},\frac{1}{2},0)$.

In Fig. 3 we have shown points within and on the boundary having special symmetry. Of those within the fcc Brillouin zone, the points Γ, X, L, W have the symmetry O_h, C_{1h}, D_{3d}, and D_{2d}, respectively. The character tables and irreducible representations can be found in Ref. 4. The other case C_{4v}^{12} is somewhat more complicated since it is nonsymmorphic, i.e., because of the existence of nonprimitive translations in the

TABLE III. Characters for the irreducible representations at Γ and along Δ for C_{4v}^{12}.

C_{4v}^{12}		A_1	A_2	B_1	B_2	E
E	$(I,0)$	1	1	1	1	2
C_4^2	$(\delta_{2z},0)$	1	1	1	1	−2
C_4	(δ_{4z}, t_B+t_c) $(\delta_{4z}^{-1}, t_B+t_c)$	1	1	−1	−1	0
σ_v	$(\rho_y, 2t_c)$ $(\rho_x, 2t_c)$	1	−1	1	−1	0
σ_d	$(\rho_{x\bar{y}}, t_A+t_c)$ (ρ_{xy}, t_A+t_c)	1	−1	−1	1	0

[4] G. F. Koster, in *Solid State Physics*, edited by F. Seitz and D. Turnbull (Academic Press Inc., New York, 1957), Vol. 5, p. 173.

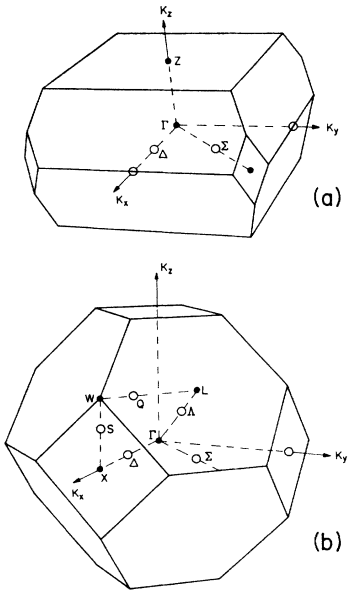

FIG. 3. The first Brillouin zone of (a) body-centered tetrogonal structure, and (b) fluorite structure.

symmetry operations, the dimensionalities of the irreducible representations and the whole nature of these representations for some of the symmetry points on the Brillouin-zone boundary are quite different from those suggested by the ordinary representations found for the group of the wave vector. For the present purpose, we are primarily interested in the band edge which is at the center of the Brillouin zone. Therefore, we shall not elaborate the details of symmetry of space group C_{4v}^{12}. We only give the character table and the irreducible representations at point Γ and along the $\langle 001 \rangle$ direction (excluding the point Z) for C_{4v}^{12} (Table III).

III. COMPUTATIONAL PROCEDURE

As is well known, in the pseudopotential formalism[5] the pseudo-Hamiltonian may be expressed as the sum of kinetic energy and pseudopotential energy parts:

$$H' = T + V_{\text{ps}}(\mathbf{r}). \tag{3.1}$$

$V_{\text{ps}}(\mathbf{r})$ is, in turn, expressed as the sum of the atomic pseudopotentials for atoms in the crystal

$$V_{\text{ps}}(\mathbf{r}) = \sum_{b,i} V_{\text{ps}}^{(b)}(\mathbf{r} - \mathbf{R}_{bi}). \tag{3.2}$$

The index b denotes the type of atom and the index i refers to the atomic site with position vector $\mathbf{R}_{bi}$. The matrix elements of (3.2) between the plane-wave states can be accurately determined as

$$\langle \mathbf{k} | V_{\text{ps}}(\mathbf{r}) | \mathbf{k}' \rangle = \sum_b [V_{\text{ps}}^{(b)}(\mathbf{q}) S_b(\mathbf{q}) \delta_{\mathbf{k}-\mathbf{k}'-\mathbf{q}}], \tag{3.3}$$

[5] See, for instance, J. C. Phillips and L. Kleinman, Phys. Rev. **116**, 287 (1959); B. J. Austin, V. Heine, and L. J. Sham, *ibid.* **127**, 276 (1962).

where $V_{ps}^{(b)}(\mathbf{q})$ is the Fourier transform of $V_{ps}^{(b)}(\mathbf{r})$ and

$$S_b(\mathbf{q})=\sum_j e^{-i\mathbf{q}\cdot\mathbf{R}_{bj}}. \tag{3.4}$$

Since there are only two types of atoms present, we may write

$$\langle\mathbf{k}|V_{ps}^{(r)}|\mathbf{k}'\rangle=\delta_{\mathbf{k}-\mathbf{k}'-\mathbf{q}}[V_{ps}^{As}(\mathbf{q})S_{As}(\mathbf{q}) +V_{ps}^{Cd}(\mathbf{q})S_{Cd}(\mathbf{q})]. \tag{3.5}$$

Let

$$S_{Cd}(\mathbf{q})=S_{Cd^I}(\mathbf{q})-S_{Cd^{II}}(\mathbf{q}). \tag{3.6}$$

Both terms in (3.6) have the form of Eq. (3.4), but the first sum is over the Cd sites given in Fig. 2(a) and the second one over the vacant sites given in Fig. 2(b). Note that Fig. 2(a) is composed of three interpenetrated fcc lattices, the three basis atoms being at

$$\text{As: } \mathbf{r}_0=(0,0,0),$$
$$\text{Cd: } \mathbf{r}_1=(\tfrac{1}{8}a,\tfrac{1}{8}a,\tfrac{1}{8}a),$$
$$\text{Cd: } \mathbf{r}_2=(\tfrac{3}{8}a,\tfrac{3}{8}a,\tfrac{3}{8}a).$$

Therefore, from the lattice sum rule we have

$$S_{As}(\mathbf{q})=\sum_j e^{-i\mathbf{q}\cdot\mathbf{R}_j^{As}}=\delta_{\mathbf{q}\mathbf{G}'}\Omega N, \tag{3.7}$$

$$S_{Cd^I}(\mathbf{q})=\sum_j e^{-i\mathbf{q}\cdot\mathbf{R}_j^{Cd}}=\sum_j e^{-i\mathbf{q}\cdot\mathbf{R}_j^{As}}(e^{-i\mathbf{q}\cdot\mathbf{r}_1}+e^{-i\mathbf{q}\cdot\mathbf{r}_2})$$
$$=(e^{-i\mathbf{q}\cdot\mathbf{r}_1}+e^{-i\mathbf{q}\cdot\mathbf{r}_2})\delta_{\mathbf{q}\mathbf{G}'}\Omega N, \tag{3.8}$$

where N is the number of unit cells in the crystal, Ω is the volume of the cell, and $\mathbf{G}'$ has the meaning given in Eq. (2.4). From Eq. (3.5) to Eq. (3.8), we obtain

$$\langle\mathbf{k}|V_{ps}(\mathbf{r})|\mathbf{k}'\rangle=\delta_{\mathbf{k}-\mathbf{k}'-\mathbf{G}'}\{V_{ps}^{As}(\mathbf{G}')+2V_{ps}^{Cd}(\mathbf{G}') \times\cos[\tfrac{1}{4}a(q_x+q_y+q_z)]\cos[\tfrac{1}{2}a(q_x+q_y+q_z)]\} -V_{ps}^{Cd}(\mathbf{q})S_{Cd^{II}}(\mathbf{q})\delta_{\mathbf{k}-\mathbf{k}'-\mathbf{q}}. \tag{3.9}$$

Here we want to point out that Eq. (3.9) is an exact expression for the structure given in Fig. 2. If we can carry out the calculation using Eq. (3.9), we would obtain the band structures of the Cd_3As_2 crystal with C_{4v}^{12} symmetry. However, as some of the discussions in previous sections indicate, there are some difficulties in performing the computation in its exact form Eq. (3.9). If we evaluate $S_{Cd^{II}}(\mathbf{q})$ according to the structure shown in Fig. 2(b), several difficulties arise:

(1) Because of the nonsymmorphic character of Fig. 2(b) $S_{Cd^{II}}(\mathbf{q})$ becomes a complex function. Thus the matrix element Eq. (3.9) is also complex.

(2) $S_{Cd^{II}}(\mathbf{q})$ will contain a factor $\delta_{\mathbf{q}-\mathbf{G}}$, where G's are RLV given by Eq. (2.3). There are 89 RLV, G' with $|\mathbf{G}'|\leq 8.7(2\pi/a)$, but the number of RLV, G with $|\mathbf{G}|\leq 8.7(2\pi/a)$, is 2780. This means that the presence of the sum over vacant sites enlarges the order of the secular determinant in the calculation by a factor of 30 in order to reach the same degree of convergence.

In view of these difficulties, we feel that a physically realistic approximation such as described in Sec. II must be employed in our present calculation. In doing so, $S_{Cd^{II}}(\mathbf{q})$ is replaced by $S'(\mathbf{q})$. It is clear that the averaged structure factor of the vacancy structures which contain only small cubes of the same orientation is $S'(\mathbf{q})=\frac{1}{4}S_{Cd^I}(\mathbf{q})$. Consequently,

$$V_{ps}^{Cd}(\mathbf{q})S'(\mathbf{q})=\tfrac{1}{4}V_{ps}^{Cd}(\mathbf{q})S_{Cd^I}(\mathbf{q}), \tag{3.10}$$

and Eq. (3.9) reduces to

$$\langle\mathbf{k}|V_{ps}(\mathbf{r})|\mathbf{k}'\rangle=\delta_{\mathbf{k}-\mathbf{k}'-\mathbf{G}'}\{V_{ps}^{As}(\mathbf{G}') +\tfrac{3}{2}V_{ps}^{Cd}(\mathbf{G}')\cos[\tfrac{1}{4}a(q_x+q_y+q_z)] \times\cos[\tfrac{1}{2}a(q_x+q_y+q_z)]\}. \tag{3.11}$$

The matrix element in Eq. (3.11) can readily be evaluated once the atomic pseudopotentials are chosen.

It is interesting to see that Eq. (3.11) may be explained, alternatively, as having the same structure factors as a fluorite structure while the Cd potential in the curly bracket of Eq. (3.9) is replaced by $\frac{3}{4}$ that of Cd potential. The effective number of valence electrons in this fluorite unit cell is now eight, of which five belong to As $4s^24p^3$ and three belong to Cd $5s$ levels.

As regards the atomic pseudopotentials, we use the local pseudopotentials determined in Refs. 2 and 3 with volume correction factor. The crystal pseudopotential form factor in the right-hand side of Eq. (3.11) is expressed in Table II for several given values of $\mathbf{G}'$. In our calculations for Zn_3As_2 and $Zn_{1.8}Cd_{1.2}As_2$, we again use Eq. (3.11) but allow the change in lattice parameters and replace $V_{ps}^{Cd}(\mathbf{G}')$ by $V_{ps}^{Zn}(\mathbf{G}')$ and $\frac{1}{3}[1.8V_{ps}^{Zn}(\mathbf{G}')+1.2V_{ps}^{Cd}(\mathbf{G}')]$, respectively, in each case.

The calculation of the band structure was carried out in a fashion similar to that described in Ref. 3. Ninety plane waves were used in the expansion of the pseudowave functions. For reasons of economy, the secular determinants are solved using Löwdin's perturbation technique.[6] The complete band structures along several symmetry directions for Cd_3As_2, $Cd_{1.2}Zn_{1.8}As_2$, and Zn_3As_2 in their hypothetical structures are given in Figs. 4–6.

IV. RESULTS

The over-all band structures of Cd_3As_2, Zn_3As_2, and $Zn_{1.8}Cd_{1.2}As_2$ are shown in Figs. 4, 5, and 6, respectively. Spin-orbit couplings and other relativistic effects are not included in these calculations. It can be seen that they all resemble the band structures of the III-V compounds InAs, GaSb,[7] etc., as we would expect. The lowest valence band belongs to an arsenic s-like level. The second band is a Cd (Zn) s-like band. The third and fourth bands are s-like about Cd, and p-like about As atoms.

[6] P. Löwdin, J. Chem. Phys. **19**, 1396 (1951).
[7] M. L. Cohen and T. K. Bergstresser, Phys. Rev. **141**, 789 (1966).

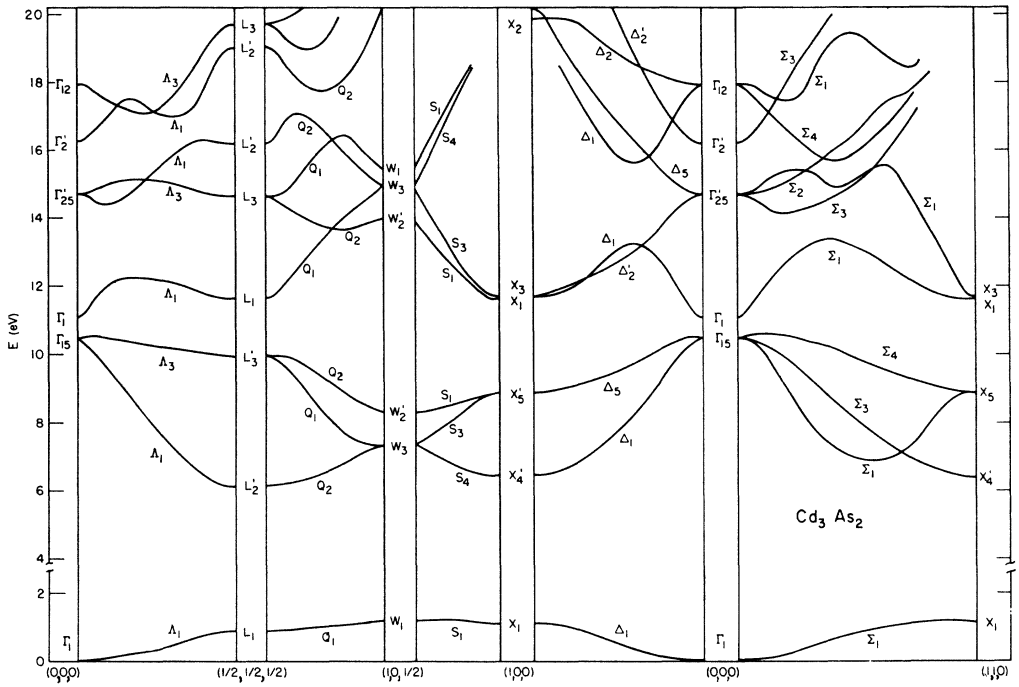

FIG. 4. Energy bands of Cd_3As_2 in its hypothetical crystal structure.

The valence-band maxima of Cd_3As_2 occur along ⟨100⟩ and ⟨110⟩ directions at points (0.065, 0, 0) and (0.125, 0.125, 0) close to the center of the Brillouin zone. The maximum of Σ_4 is only 0.15 eV higher than Γ_{15} in energy. On the other hand, the direct gap at Γ point is 0.6 eV. The conduction-band minimum at Γ has a very small effective mass. Our calculated value is $m_e^*=0.045m_0$ as compared with the experimental

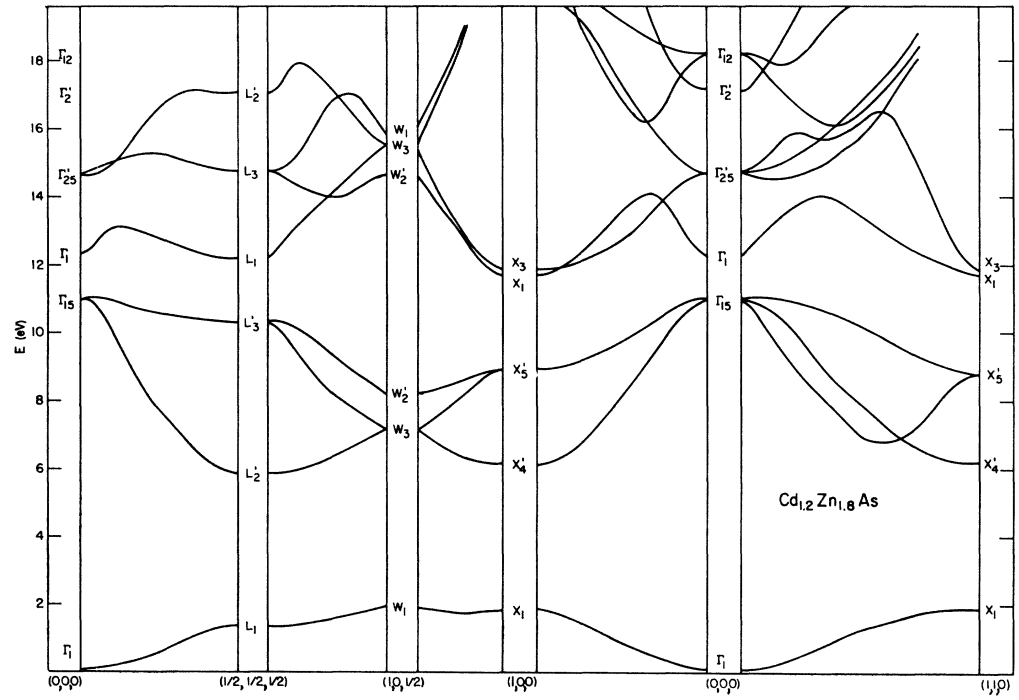

FIG. 5. Energy bands of $Cd_{1.2}Zn_{1.8}As_2$.

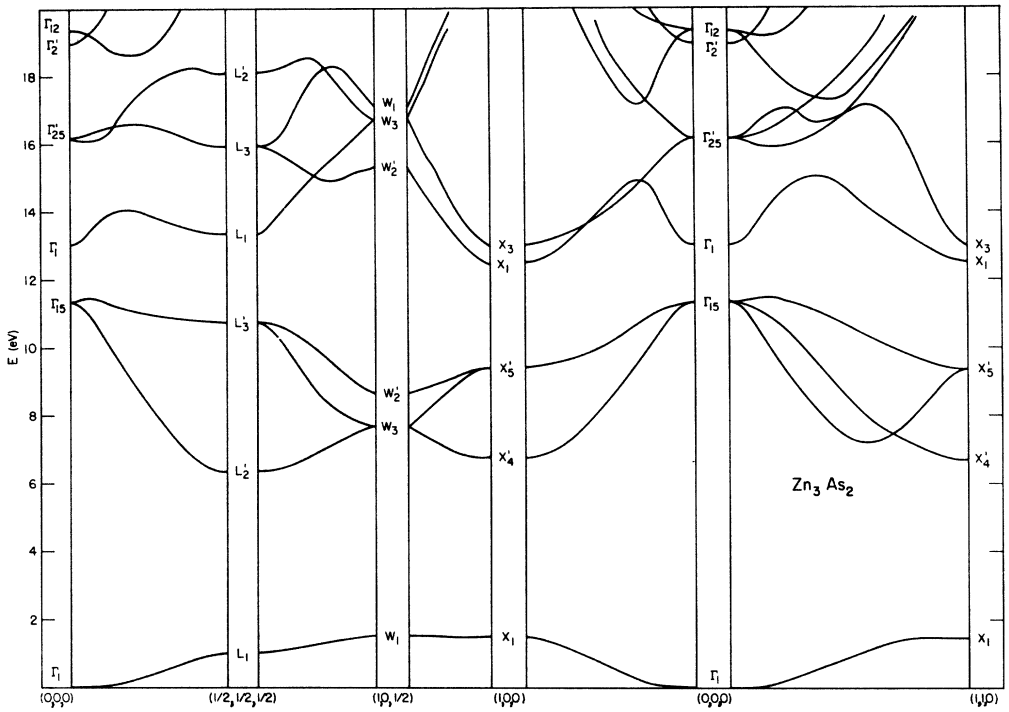

FIG. 6. Energy bands of Zn_3As_2.

value of $0.041m_0$.[8] The light-hole effective mass appears to be only slightly greater than that of the electron.

In Figs. 5 and 6 the conduction-band minima are located at X rather than at Γ. The X and Γ points are, in fact, equivalent points in a real crystal structure; therefore, we can still consider the forbidden energy gaps to be close to the center of the Brillouin zone. The effective mass for Zn_3As_2 at X_1 is calculated to be $m_e^*=0.126m_0$.

We list several interband energy differences for these materials in Table IV.

Experimental reflection spectra were recently studied for these II-V compounds in the range 1–12 eV.[9,10] The structure of the spectra is quite similar to that of III-V compounds.[11] We list several prominent reflectivity peaks in Table IV. It has been shown that in III-V compounds the E_1 peak corresponds to the transition $\Lambda_3^v \rightarrow \Lambda_1^c$, where the superscripts refer to valence and conduction bands. The Λ point is, in fact, very close to L. It is interesting that this is also true in our results. We have peaks at 1.8 and 2.6 eV compared with 1.7 and 2.1 eV in the experimental data. The next peak E_2 corresponds to the $X_5^v \rightarrow X_1^c$ transition for the III-V compounds. Our results for $X_5' \rightarrow X_1$ for Cd_3As_2 and Zn_3As_2, 3.0 and 3.2 eV, are also close to the experimental data 3.65 and 3.5 eV, respectively. The E_3 peak, formerly identified to be associated with the transition $L_3^c \rightarrow L_3^v$ in GaAs, also agrees with $L_3' \rightarrow L_3$ transition in our case. Our calculated value for this transition for Cd_3As_2 is 4.7 eV. Considering the similarity in both band structures and reflection spectra of these II-V and III-V compounds, we may anticipate that the transition assignments we made are quite reasonable. There are frequently more than one critical point contributing to each prominent peak in the optical spectra. We discuss only the ones at high symmetry

TABLE IV. Calculated interband energy differences and observed reflectivity peaks (all entries in eV).

	Cd_3As_2	Zn_3As_2	$Cd_{1.2}Zn_{1.8}As_2$
$L_3' \rightarrow L_1$	1.8	2.6	1.9
$X_5' \rightarrow X_1$	3.0	3.2	2.8
$L_3' \rightarrow L_3$	4.7	5.2	
$\Gamma_{15} \rightarrow \Gamma_1$	0.6	1.65	1.3
$\Gamma_{15} \rightarrow X_1$	1.2	1.1	0.7
E_1[a]	1.7	2.1	
E_2[a,b]	3.65	3.5	
E_3[b]	4.5		

[a] See Ref. 9.
[b] See Ref. 10.

[8] E. D. Haidemenakis, M. Balkanski, E. D. Palik, and J. Tavernier, J. Phys. Soc. Japan Suppl. **21**, 189 (1966).
[9] V. V. Sobolev, N. N. Syrba, and S. D. Shutov, in *Chemical Bonds in Semiconductors and Thermodynamics*, edited by N. N. Sirota (Consultants Bureau, New York, 1968), p. 165.
[10] J. R. Stevenson (private communication).
[11] D. L. Greenaway and M. Cardona, in *Proceedings of the International Conference on the Physics of Semiconductors, Exeter, 1962* (The Institute of Physics and The Physical Society, London, 1962), p. 666; M. Cardona, K. L. Shaklee, and F. H. Pollak, Phys. Rev. **154**, 696 (1967).

points of the fluorite Brillouin zone, which are also symmetry points of the real Brillouin zone.

V. BAND-EDGE STRUCTURES OF Cd_3As_2, Zn_3As_2 AND THEIR MIXED CRYSTALS

After we have the energy-band structures of the II-V compounds in their hypothetical structure, it is important to examine what we would expect for the band structures in the real crystals. Let us consider the effect of the small residual potential which is the difference between the potential we used in our calculation and the potential for the real crystal. As we have mentioned at the end of Sec. II, this residual potential, having the symmetry of C_{4v}[12], is very small and difficult to evaluate quantitatively. We can only estimate its effect qualitatively to give a picture of the band-edge structures for the real crystals.

The small residual potential, which acts upon the electrons in the fluorite structure, will tend to mix states which have wave numbers differing by the RLV of the real structure and will have negligible effect except when the unperturbed states that are mixed have very small energy difference. Among the states which will have significant alteration in energy, we choose to discuss only the states near to band edges.

X_1 and Γ_1, at the bottom of the conduction bands, both have s-like symmetry in the real crystals. They have energy difference $E(X_1)-E(\Gamma_1)=0.5$ eV in Cd_3As_2. In such condition they will interact via the small residual potential and, as a result, push each other apart. The perturbed Γ_1 and X_1 levels belong to the identity representation A_1 in the real structure (see Table III) and one of them moves to higher-energy position, the other to lower-energy position. The residual potential and the spin-orbit interaction both will lift the degeneracy of Γ_{15}. The Γ_{15} state is p-like about As atoms. Since the spin-orbit splitting for free As atoms is only approximately 0.3 eV, the separation between the split-off Γ_{15} bands will be 0.35 eV. The interaction between X_5' and Γ_{15} via the residual potential will also help to raise the valence-band maximum. The total effect is estimated to raise the conduction-band minimum in an amount 0.2 eV and lower the valence-band maximum by the same amount for the case of Cd_3As_2. At this point, we may tentatively construct the band-edge structures for the real crystal, a schematic diagram of which is presented in Fig. 7. The predicted forbidden energy gap E_g for Cd_3As_2 in the real structure is $\sim$0.2 eV or even smaller; perhaps a grey Sn-type zero-gap structure may appear.[12] The E_g for Zn_3As_2 in the real structure is close to 0.9 eV and that for $Cd_{1.2}Zn_{1.8}As_2$ is close to 0.4 eV. Both gaps are between $A_1(X_1)$ and $E(\Gamma_{15})$ at the center of the Brillouin zone of the real crystal structure. The electron effective mass for Zn_3As_2, $0.21m_0$, is much greater than

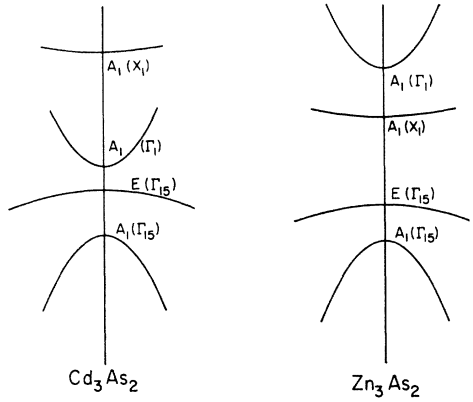

FIG. 7. Schematic diagram of predicted band-edge structures of (a) Cd_3As_2, and (b) Zn_3As_2 in their real crystal structure. The states are labeled by the irreducible representations of the C_{4v}[12] factor group and the corresponding representations of the fluorite structure from which the new states are formed.

that of Cd_3As_2. This is mainly because the conduction-band minima originate from different states for these two cases.

When the residual potential acts on the point L, the point L will be mixed with states at the midpoints between ΓX in (100) and (110) directions. The new perturbed states are at the Brillouin-zone boundary of the real structure. According to Figs. 4–6, only the L_3' level has states Δ_5 and Σ_4 at $(4\pi/a)(\frac{1}{2},0,0)$, $(4\pi/a)(\frac{1}{2},\frac{1}{2},0)$ near to it and, hence, will change its energy slightly. This may help to decrease the energies of the transitions $L_3'\rightarrow L_1$ and $L_3'\rightarrow L_3$ and bring them into better agreement with experimental E_1, E_3 peaks. The X_5' level is pushed down by its interaction with Γ_{15} and hence the $X_5'\rightarrow X_1$ transition will increase in energy. This also helps to approach the experimental E_2 peak as given in Table IV. For the sake of completeness, we summarize other available experimental information to see how our present result might interpret some of the data.

Besides the aforementioned reflectivity measurements, there have been transmission and reflection measurements in thin film Cd_3As_2 over the range 0.1–1.2 eV. Zdanowicz[13] observed extremely high values of the absorption coefficient α at about 0.6 eV and a decrease of α by two orders of magnitude within a narrow region of frequencies. He suggested that 0.6 eV can be taken as the energy gap for direct transitions. A second decrease of the absorption coefficient at 0.13 eV by about one order of magnitude is then attributed to the occurrence of indirect transitions. Interband magneto-optical (IMO) studies of Cd_3As_2 [8] also reveal a very small energy gap $\sim$0.025 eV, an electron effective mass of $0.041m_0$, and a valence-band effective mass of $0.12m_0$. Armitage and Goldsmid[14] explain the optical

[12] R. J. Wagner, E. D. Palik, and E. S. Swiggard, Phys. Letters **30A**, 175 (1969).

[13] L. Zdanowicz, Phys. Status Solidi **20**, 473 (1967).

[14] D. Armitage and H. J. Goldsmid, Phys. Letters **28A**, 149 (1968).

work in terms of a Kane-type band with a small direct gap, an indirect overlap, and a large Burstein-Moss shift. An alternative band structure was suggested by Wagner *et al.*[12] to explain the observation of IMO transitions in mixed $Cd_xZn_{3-x}As_2$ crystals as a function of composition. They suggest an α-Sn-like zero-band-gap model for Cd_3As_2. Our present calculation predicts a band structure in favor of the latter model. As shown in Fig. 7, the energy gap is at the center of the Brillouin zone. The $A_1 \rightarrow E$ is the small direct gap less than 0.2 eV. However, we have a different interpretation for the 0.6-eV transition, which was assumed to be due to the light-valence to conduction-band transition in Ref. 12. From the distinctly different absorption coefficients observed for the 0.13- and 0.6-eV transitions, we believe that the 0.6-eV transition is due to the heavy valence band $E(\Gamma_{15})$ to the higher conduction band $A_1(X_1)$ (see Fig. 7), because this is an allowed transition with stronger oscillator strength. Sexer[15] also predicts two conduction bands with effective masses $0.06m_0$ and $0.12m_0$, respectively, in order to explain the magneto-resistance results. It is surprising to see that we also have two conduction bands with effective masses similar to her results. She predicts that the two bands are separated by 0.15 eV. However, it seems impossible to have such a small energy separation for pure Cd_3As_2 from our calculated result. For the mixed crystal, the separation of the two conduction bands becomes smaller and reversal of these two bands eventually occurs.

The experimental information for Zn_3As_2 and the mixed crystals is not as complete as that for Cd_3As_2. If our interpretation for the absorption measurement for Cd_3As_2 is correct, then, because of the reversal of the two conduction bands in Zn_3As_2, we would expect to observe a strong-edge–type followed by a weak-edge–type increase of absorption as the photon energy is increased from 0.7 to 1.4 eV. Also, we expect many phenomena relating to the conduction band edge property to be significantly different from those in Cd_3As_2. More experimental investigations of the optical and electrical properties of Zn_3As_2 and a whole series of mixed crystals $Cd_xZn_{3-x}As_2$ are desirable to help establish the real energy-band structures.

[15] N. Sexer, Phys. Status Solidi **21**, 225 (1967).

ACKNOWLEDGMENTS

The author wishes to thank Dr. R. F. Wallis and Dr. S. Teitler for their helpful discussion on the manuscript, and Dr. J. R. Stevenson and Dr. R. J. Wagner for communicating their results prior to publication.

PHYSICAL REVIEW VOLUME 188, NUMBER 3 15 DECEMBER 1969

Coupling of LO and TA Phonons to the 1.39-eV Broad-Band Luminescent Center in GaAs:Zn†

DAVID K. BRICE

Sandia Laboratories, Albuquerque, New Mexico 87115

(Received 26 May 1969; revised manuscript received 25 August 1969)

The phonon structure accompanying the broad-band luminescence spectrum centered at 1.39 eV in GaAs:Zn at 4.2°K has been analyzed to obtain the low-temperature coupling strengths S of both LO and TA phonons to the center. Values of $S(\mathrm{LO})=0.439$ and $S(\mathrm{TA})=0.818$ are obtained. The value of $S(\mathrm{LO})$ is then used in a procedure developed by Hopfield to limit the geometrical extent of the exciton responsible for the luminescence. In the Appendix, Hopfield's procedure is used to obtain formulas for the coupling strength $S(\mathrm{LO})$ for charge densities composed of electron-hole pairs. The results of this calculation are pertinent not only to phonon coupling to exciton charge distributions, but also to coupling to donor-acceptor-pair charge distributions.

I. INTRODUCTION

RECOMBINATION radiation is often one of the most important probes available for the determination of properties of localized impurity or defect states in a solid. When the recombination luminescence is accompanied by phonon emission, further information can often be obtained concerning the nature of the localized state.

The important parameter describing the interaction of the phonons and the luminescent center is the coupling strength parameter S. The value of this parameter is the average number of phonons emitted accompanying the luminescence, with the probability for emission of different numbers of phonons following a Poisson distribution. Hopfield[1] has shown how the coupling strength S for longitudinal optical (LO) phonons interacting with a localized charge distribution in ionic crystals can be related to the "size" of the charge distribution. Determination of S for LO phonons then allows an estimate to be made of how tightly bound a luminescent center is.

† Work supported by the U. S. Atomic Energy Commission.

[1] J. J. Hopfield, J. Phys. Chem. Solids **10**, 110 (1958).